Construction and Building Materials 254 (2020) 119293

Contents lists available at ScienceDirect

Construction and Building Materials

journal homepage: www.elsevier.com/locate/conbuildmat

A calibration of the material model for FRC

Duc-Kien Thai [a,*], Duy-Liem Nguyen [b], Duy-Duan Nguyen [c]

[a] Department of Civil and Environmental Engineering, Sejong University, 98 Gunja-dong, Gwangjin-gu, Seoul 143-747, South Korea
[b] Department of Civil Engineering and Applied Mechanics, Ho Chi Minh City University of Technology and Education, 1 Vo Van Ngan St., Thu Duc District, Ho Chi Minh City, Viet Nam
[c] Department of Civil Engineering, Vinh University, Vinh 461010, Viet Nam

HIGHLIGHTS

- An adequate calibration of a constitutive material model for FRC is developed.
- Based on experimental data, typical structural behaviors of FRC are discussed.
- Numerical analyses are performed to evaluate the performance of the calibrated model.
- Calibrated parameters used for FRC are provided for relevant studies.

ARTICLE INFO

Article history:
Received 8 July 2019
Received in revised form 24 February 2020
Accepted 20 April 2020

Keywords:
Fiber reinforced concrete
Calibrated model
K&C model
Strain-rate effect
Blast loading
LS-DYNA

ABSTRACT

This paper presents a calibration of a constitutive material model, which can be applied to describe the complex static and dynamic behavior of the fiber reinforced concrete (FRC) structures subjected to static and high-rate loading conditions. The well-known K&C material model, which is MAT072r3 as executed in LS-DYNA, is employed for the purposed of this calibration. Various experimental data on tension, compression, and high-rate behaviors of FRC material using axial and tri-axial tests are used to generate the input parameters. Numerical simulation of single specimens on compression and bending subjected to static loading, and of an FRC column under blast loading are implemented to illustrate the performance of the calibrated material model. It is shown that the calibrated material model proposed in this study presents a good agreement compared to the experimental results.

1. Introduction

Fiber reinforced concrete (FRC) material has been widely used in construction due to its superiority in ameliorating the ductility and energy absorption. Especially, with high energy absorption capacity, FRC has been also used effectively in structures under extreme loading conditions such as blast and impact loading [1,2]. Therefore, more and more researches related to FRC have been conducted using both experimental, theoretical, and simulating approaches. The problem comes from the fact that, while there have been a number of material models for conventional concrete, none of the models have been developed specifically for FRC structures. While the need for numerical simulation of FRC structures has been increasing. This requires an improvement of material models relevant to the structural behavior of FRC under both static and dynamic load conditions, which is very urgent.

There are several material models for concrete which have been developed in LS-DYNA so far. Among them, three following models are usually used in numerical simulations of the reinforced concrete structures including Karagozian & Case Concrete (K&C) model represented by MAT#072r3, Winfrith Concrete described by MAT#084 and Continuous Surface Cap (CSC) model as MAT#159. Advantages, disadvantages, and different simulating abilities of these models were evaluated and compared by Wu et al. [3]. The Winfrith concrete model requires a very simple input and can capture the crack pattern, however, it cannot model the softening in compression and shear dilatation, which represents the realistic behavior of concrete. The CSC model, on the other hand, can exhibit the damage and modulus reduction, but this model only appropriately describes for low confinement. And it is not easy to accurately model the strain-rate effect since it uses different strain-rate effect calibration compared to other models. Nevertheless, although the K&C model does not consider cracking pattern and damage of

* Corresponding author.
E-mail addresses: thaiduckien@sejong.ac.kr (D.-K. Thai), liemnd@hcmute.edu.vn (D.-L. Nguyen), duyduankxd@vinhuni.edu.vn (D.-D. Nguyen).

https://doi.org/10.1016/j.conbuildmat.2020.119293
0950-0618/

structures, which can alternatively use the erosion option, this model can represent most of the structural behavior of concrete-like materials. Therefore, K&C has been widely utilized for the simulation of both concrete-like and concrete materials with a large scope of characteristics.

Initially proposed by Malvar et al. [4], in recent years, K&C model has been improved and calibrated to capture the realistic behavior of different types of concrete. Release III of the K&C model improved by Magallanes et al. [5] provided an automatic input parameters generation, methods to reduce mesh-dependencies. It also gave a method to preserve fracture energy based on the results of the single or multiple-element simulation for user-defined parameters. Despite of providing a much convenience in modeling, the Release III of the K&C has limitation in providing an accurate result when applying for a wide range of different concrete types and strengths. To overcome this weakness, Markovich et al. [6] performed a modified calibration model using sets of tri-axial tests for many different types of concrete conducted by Attard and Setunge [7]. Besides, Kong et al. [8] modified the K&C model to reduce the required input parameters and enhance the prediction capacity for scabbing and cratering phenomena of structures under impact loading. Although those aforesaid improvements can provide a better performance of K&C model for the normal concrete, they are still not appropriate for concrete composite with steel fibers. In 2017, Lin and Gravina [9] calibrated this material to model the behavior of high-performance fiber reinforced concrete (HPFRC). In this work, the strain-increment effect varying from 1e-7 to 1e-5 was considered using single element tests and the damage scaling parameters were calibrated, however, other input parameters were adopted from the normal concrete, which may not describe the actual behavior of HPFRC. After that, Lin [10] continued to calibrate the K&C model for ultra-high performance fiber reinforced concrete (UHPFRC). With this work, Lin calibrated the dynamic enhanced parameters, damage scaling parameters, and damage function. However, the calibration of defined failure surfaces parameters, which controls the three failure surfaces of the material, was still missed. On the other hand, an evaluation of the strain-rate effect for FRC was carried out by Yang et al. [11]. Again, the shortcoming in the work of Yang et al. was that the failure surface parameters, damage scaling parameters, damage function, and equation of state function were adopted from the normal concrete. In general, the most significant limitation in the above-mentioned works was the lack of tri-axial test data, which directly support the calibration of the input parameters of the K&C model. Moreover, none of the given calibrations provided calibrated input parameters, which are capable of modeling of FRC. This fact gives a strong motivation to conduct this study.

To handle the limitations mentioned above, this research performs a calibration of the K&C model for modeling the complex behavior of FRC structures subjected to static and high-rate loading conditions. The model of material MAT072r3 implemented in LS-DYNA is employed to conduct this calibration. Various experimental data on tension, compression, and high-rate behaviors of FRC material using axial and tri-axial tests are used for generating the input parameters. Numerical simulations of single tests on compression and bending subjected to static loading and of an FRC column under blast loading are implemented to illustrate the performance of the calibrated material model. It is shown that the calibrated material model proposed in this study induces a good agreement compared to the experimental data.

2. Structural behavior of FRC

Fibers are added directly into concrete and mixed to create FRC, which increases the tensile strength, deformability, as well as crack distribution capacity. Using different combinations of fiber types and its content and concrete, the properties and mechanical behaviors of FRC are significantly improved compared to the conventional concrete. This section presents briefly the structural behavior of FRC under different loading conditions such as compression, tension, and high rate loading.

2.1. In compression

The compressive behavior of concrete is conventionally characterized by its stress-strain relationship. Various experimental studies, e.g. [12,13], indicated that steel fiber has considerable effects on the compressive behavior of FRC. Several series of compression tests carried out by Bencardino et al. [12] and Lee et al. [14] revealed that fiber aspect ratio, as well as fiber content, have an influence on compressive strength of FRC. It is worth noting that increasing fiber content does not seem like increasing but sometimes decreases the compressive strength of FRC [12]. However, the most important effect of the fiber is to increase the ductility of the FRC, which were indicated in all experiment studies in literature, e.g. [12,14–16]. Comparisons presented in [12] and [14] also showed that as fiber content increases, the slop of the softening branch of the stress-strain curve decreases. Obviously, like conventional concrete, the lateral pressure noticeably affects the compressive behavior of FRC. Experimental data presented in the work of Gholampour and Ozbakkaloglu [17] pointed out that an increment of lateral pressure yields a significant improvement of both ultimate and residual strength of FRC.

The comparison between the stress-strain relationship of the normal concrete, represented by the dashed curve and the FRC, represented by the continuous curve is shown in Fig. 1. For the normal concrete, the CEB-FIP [18] equation is used to specify the stress-strain curve. According to CEB-FIP, the stress-strain relationship of concrete can be approximated by the following equation

$$\sigma_c = -\frac{\frac{E_{ci}}{E_{c1}}\frac{\varepsilon_c}{\varepsilon_{c1}} - \left(\frac{\varepsilon_c}{\varepsilon_{c1}}\right)^2}{1 + \left(\frac{E_{ci}}{E_{c1}} - 2\right)\frac{\varepsilon_c}{\varepsilon_{c1}}} f_{cm} \; for \; |\varepsilon_c| < |\varepsilon_{c,\lim}| \tag{1}$$

where

E_{ci} is the tangent modulus, can be calculated by E_{ci} = $2.15 \times 10^4[f_{cm}/10]^{1/3}$,

E_{c1} is the secant modulus, can be calculated by $E_{ci1} = f_{cm}/0.0022$,

f_{cm} is the peak strength,

$\varepsilon_{c1} = -0.0022$,

$\varepsilon_{c,\lim} = -0.003$ corresponding to concrete C50,

σ_c and ε_c stand for the stress and strain, respectively.

Whereas, for FRC, the recent model proposed by Lee et al. [14] based on their test data is employed to plot the curve. Accordingly,

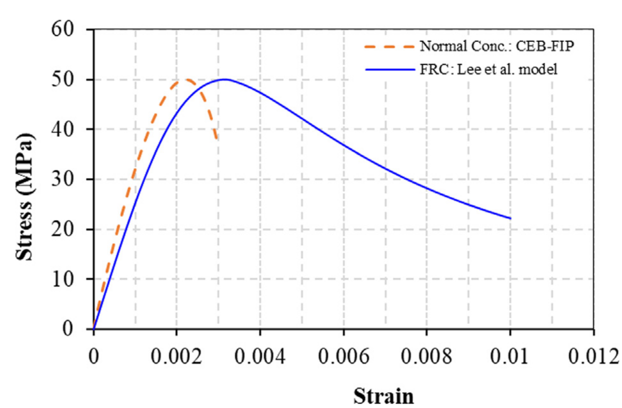

Fig. 1. Comparison of compressive stress-strain curves.

the compressive behavior of FRC can be represented by the equation as follow

$$\sigma_c = -\left[\frac{A\left(\frac{\varepsilon_c}{\varepsilon_0}\right)}{A-1+\left(\frac{\varepsilon_c}{\varepsilon_0}\right)^B}\right] f_{cm} \quad (2)$$

where A and B are parameters, which are calculated by using the following equations

- For the ascending branch, i.e. $\varepsilon_c/\varepsilon_0 \leq 1.0$

$$A = B = \frac{1}{1-\left(\frac{f_{cm}}{\varepsilon_0 E_c}\right)} \quad (3)$$

- For the descending branch, i.e. $\varepsilon_c/\varepsilon_0 > 1.0$

$$A = 1 + 0.723\left(V_f \frac{l_f}{d_f}\right)^{-0.957} \quad (4)$$

$$B = \left(\frac{f_{cm}}{50}\right)^{0.064}\left[1 + 0.882\left(V_f \frac{l_f}{d_f}\right)^{-0.882}\right] \quad (5)$$

ε_0 is the strain at peak strength, and can be determined by

$$\varepsilon_c = \left(0.0003 V_f \frac{l_f}{d_f} + 0.0018\right) f_{cm}^{0.12} \quad (6)$$

E_c is the elastic modulus of FRC, calculated by

$$E_c = \left(-367 V_f \frac{l_f}{d_f} + 5520\right) f_{cm}^{0.41} \quad (7)$$

and V_f and l_f/d_f are the fiber volume fraction and fiber aspect ratio, respectively.

It is clearly shown that with the same compressive strength, the strain at peak strength as well as the ultimate strain of FRC are much higher than those of normal concrete. As a result, compressive behavior is more ductile than the behavior of normal concrete. This is the main difference of the compressive characteristic between the two materials.

2.2. In tension

The main influence of the fiber is to improve the multi-cracking and strain hardening properties of FRC [19–22]. That formation of multiple small cracks increases the ductility, deformability, and energy absorption. Due to the distribution of multi-cracking, the tensile strain capacity is significantly increased. The tensile behavior of FRC, therefore, is much different from the normal concrete.

Naaman [23] classified the tensile behavior response of FRC into two cases, namely, strain-softening or strain-hardening, based on their stress-strain response as presented in Fig. 2. In the strain-softening case (curve I), the stress-strain curve exhibits the linear relationship until the first cracking occurs. Localization then occurs immediately after first cracking. Due to the increase of elongation, the stress after first cracking is smaller than that at first cracking. The softening part of the stress-strain curve exhibits the softening behavior until the stress goes to zero. In the strain-hardening case (curve II), the stress after first cracking keeps increasing with strain, and multiple cracking occurs up to the maximum post-cracking stress. The first cracking strength can be calculated as

$$\sigma_{cc} = f_{ctm}(1 - V_f) + \alpha\tau V_f\left(\frac{l_f}{d_f}\right) \quad (8)$$

and the post-cracking strength can be determined by

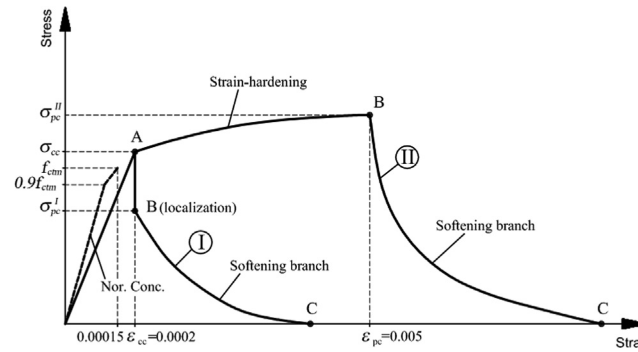

Fig. 2. Tensile stress-strain curves of normal concrete and FRC.

$$\sigma_{pc} = \lambda\tau V_f\left(\frac{l_f}{d_f}\right) \quad (9)$$

where f_{ctm} is the tensile strength of the matrix; τ stands for the bond strength; α and λ describes coefficients. If $\sigma_{cc} > \sigma_{pc}$ then strain-softening occurs, if $\sigma_{cc} \leq \sigma_{pc}$, strain-hardening occurs.

Comparison of tensile behaviors between FRC and normal concrete with the same matrix strength of C50 according to CEB-FIP [18] is also shown in Fig. 2. It is noted that the CEB-FIP model is applied for the normal concrete to determine its stress-strain curve. Obviously, FRC is much more ductile than the normal concrete, which governs a different structural behavior between the two materials.

2.3. High strain-rate effect

Many experimental studies showed that the mechanical properties of FRC sensitively affect the strain rate in both compression [24–26] and tension [1,2,27]. Tensile and compressive strengths of FRC increases as the strain rate increases. Commonly, a dynamic increment factor (DIF) is used as the ratio of dynamic to static strengths of the material. The matrix strength, fiber type, and fiber content were found to have an influence on the rate sensitivity of FRC. The influence of different parameters on the tensile strength of FRC is shown in Fig. 3. It is evident from the work of Wang et al. [28] that the matrix strength had some effect on the tensile strength of FRC as shown in Fig. 3a. Similarly, the different fiber types showed different strain sensitivity as demonstrated in the work of Xu et al. [26] (see Fig. 3b). However, the test data provided by Sun et al. [29] indicated that fiber content does not has any significant effect on strain sensitivity as shown in Fig. 3c.

In the same trend, the test data carried out by Park et al. [2] and Kim et al. [1] demonstrated that matrix strength and fiber type have pronounced effects on the rate sensitivity of FRC tensile strength, as shown in Fig. 4a and 4b, respectively. Whereas, fiber volume fraction produces a trivial effect on the DIF, as shown in Fig. 4c. In addition, it emphasizes that matrix strength and fiber type should be taken into account when estimating the DIF, but not fiber content.

For predicting the DIF for the normal concrete, CEB-FIP design code [18] provides formulas as follows:

In compression:

$$DIF = \begin{cases} (\dot{\varepsilon}_c/\dot{\varepsilon}_{co})^{1.026\alpha_s} & for\ |\dot{\varepsilon}_c| \leqslant 30s^{-1} \\ \gamma_s(\dot{\varepsilon}_c/\dot{\varepsilon}_{co})^{1/3} & for\ |\dot{\varepsilon}_c| > 30s^{-1} \end{cases} \quad (10)$$

In tension:

$$DIF = \begin{cases} (\dot{\varepsilon}_{ct}/\dot{\varepsilon}_{cto})^{1.016\delta_s} & for\ |\dot{\varepsilon}_{ct}| \leqslant 30s^{-1} \\ \beta_s(\dot{\varepsilon}_{ct}/\dot{\varepsilon}_{cto})^{1/3} & for\ |\dot{\varepsilon}_c| > 30s^{-1} \end{cases} \quad (11)$$

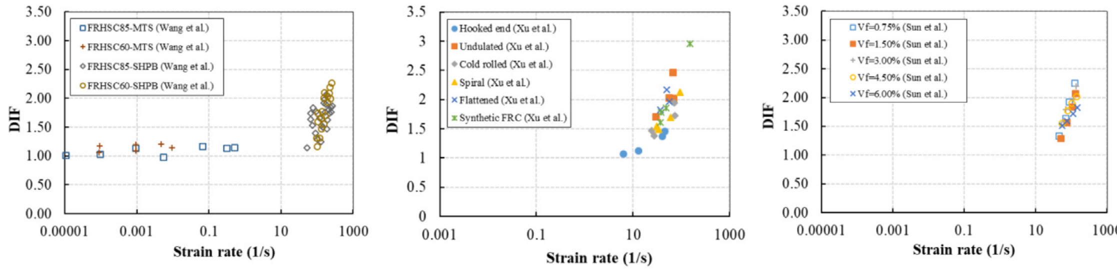

(a) Matrix strength (b) Fiber type (c) Fiber content

Fig. 3. Effect of different parameters on tensile strength of FRC.

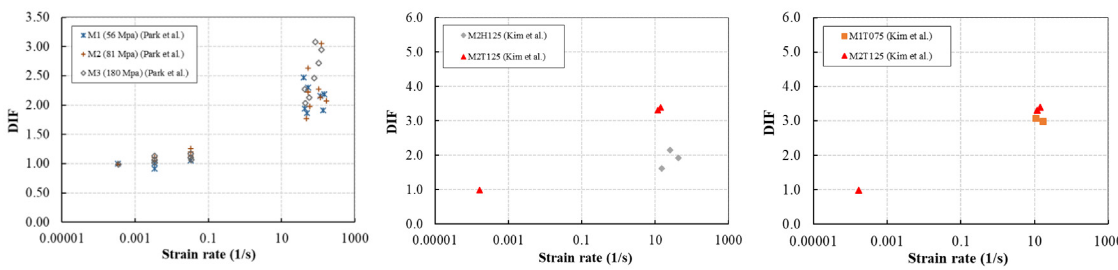

(a) Matrix strength (b) Fiber type (c) Fiber content

Fig. 4. Effect of different parameters on the compressive strength of FRC.

where $\dot{\varepsilon}_c$ and $\dot{\varepsilon}_{tc}$ are the current strain rates; $\dot{\varepsilon}_{co} = 3\times10^{-5}s^{-1}$ and $\dot{\varepsilon}_{cto} = 3\times10^{-6}s^{-1}$ are the static strain rates for compression and tension, respectively; $\alpha_s = \frac{1}{5+9f_{cm}/10}$ and $\delta_s = \frac{1}{10+6f_{cm}/10}$, here f_{cm} is the compressive strength of concrete; $\log\gamma_s = 6.15\alpha_s - 2$; $\log\beta_s = 7.112\delta_s - 2$.

However, the previous studies showed that the CEB-FIP formula is not suitable FRC [11]. Therefore, alternative formulas are needed for determining the DIF of FRC. Several models have been proposed in recent years. Among these, the following equations are found to be suitable for calculating the DIF for FRC, which are supported by test data.

In compression, the DIF formula proposed by Wang et al. [25] is expressed as

$$DIF = \begin{cases} (\dot{\varepsilon}_{ct}/\dot{\varepsilon}_{cto})^{1.016\delta_s} \; for \; |\dot{\varepsilon}_{ct}| \leqslant (30+23)s^{-1} \\ \eta(\dot{\varepsilon}_{ct}/\dot{\varepsilon}_{cto})^{\kappa} \; for \; |\dot{\varepsilon}_{c}| > (30+23)s^{-1} \end{cases} \tag{12}$$

where $\alpha_s = \frac{1}{5+9f_{cm}/10}$; $\eta = \gamma_s(1-0.3392)$ with $\log\,\gamma_s = 6.156\alpha_s - 2$; and $\kappa = (1+0.05i)/3$ with i = 1.0 for FRC.

In tension, the DIF formula proposed by Tran & Kim [27] for FRC with Twisted fiber is expressed as

$$DIF = \begin{cases} (\dot{\varepsilon}_{ct}/\dot{\varepsilon}_{cto})^{h\delta_s} \; for \; |\dot{\varepsilon}_{ct}| \leqslant 1s^{-1} \\ \beta(\dot{\varepsilon}_{ct}/\dot{\varepsilon}_{cto})^{k/3} \; for \; |\dot{\varepsilon}_{c}| > 1s^{-1} \end{cases} \tag{13}$$

where $\dot{\varepsilon}_{cto} = 10^{-6}s^{-1}$ is the static strain rate; k = 0.8 and h = 1.3 are for Twisted fiber; $\delta = 1/(1+6f_{cm}/10)$; and $\log\beta = 6h\delta - 2$.

Whereas, for Hooked fiber, the DIF formula proposed by Park et al. [2] is found to be suitable, which is given by

$$DIF = \begin{cases} (\dot{\varepsilon}_{ct}/\dot{\varepsilon}_{cto})^{\delta} \; for \; |\dot{\varepsilon}_{ct}| \leqslant 25s^{-1} \\ \beta(\dot{\varepsilon}_{ct}/\dot{\varepsilon}_{cto})^{\eta} \; for \; |\dot{\varepsilon}_{c}| > 25s^{-1} \end{cases} \tag{14}$$

where $\dot{\varepsilon}_{cto}$ is the static strain rate; $\delta = 0.017 - 27226(f_{cm}/10)^{-7.33}$; $\log\beta = -0.007082f_{cm} - 2.08$; and $\eta = 0.1208f_{cm}^{0.2622}$.

Fig. 5 compares the DIF curves between CEB-FIP model and Wang's model in compression (see Fig. 5a), and Tran & Kim's model for Twisted and Park's model for Hooked fiber in tension (see Fig. 5b).

3. K&C Material model

The developed and improved K&C material model of Malvar et al. [4,30] is a three-invariant model, which can completely consider the plasticity, strain-rate effects, and damage based on the three independent strength surfaces. Accordingly, three specific points corresponding to yield (Pt. 1), maximum (Pt. 2), and residual (Pt. 3) strengths are determined using the typical stress-strain relationship of compression test of concrete, as shown in Fig. 6. These three points represent three failure surfaces of the material. It should be noted that the stress-strain behavior of concrete is varied as a function of pressure. Fig. 7 shows the three independent shear surfaces representing the hydrostatic pressure functions.

3.1. Three failure surfaces

The yield strength surface, maximum strength surface, and residual strength surface which are described as $\Delta\sigma_y$, $\Delta\sigma_m$, and $\Delta\sigma_r$, respectively, are expressed by the functions of pressure as

$$\Delta\sigma_y = a_{0y} + \frac{p}{a_{1y} + a_{2y}p} \tag{15}$$

$$\Delta\sigma_m = a_0 + \frac{p}{a_1 + a_2p} \tag{16}$$

$$\Delta\sigma_r = \frac{p}{a_{1f} + a_{2f}p} \tag{17}$$

where $p = -(\sigma_1 + \sigma_2 + \sigma_3)/3$ describes the pressure, here, stresses are positive in tension and vice versa; a_{ij} are the defined failure surfaces parameters, which are obtained based on the tri-axial compression experimental data.

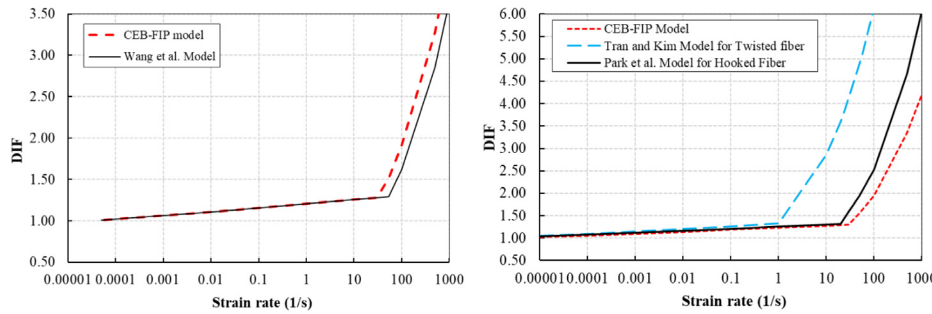

(a) In compression (b) In tension

Fig. 5. DIFs for FRC material.

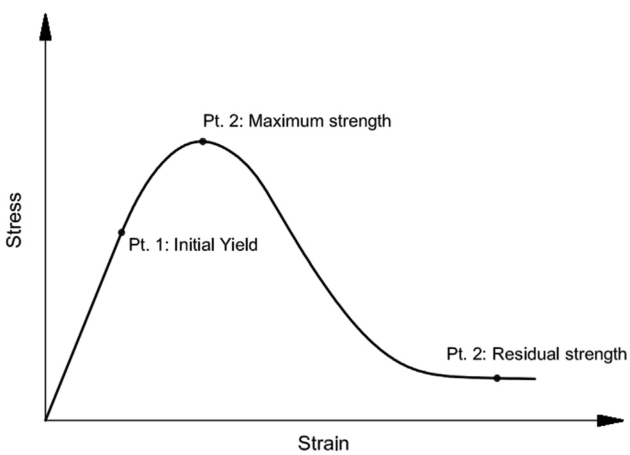

Fig. 6. Typical stress-strain curve of concrete.

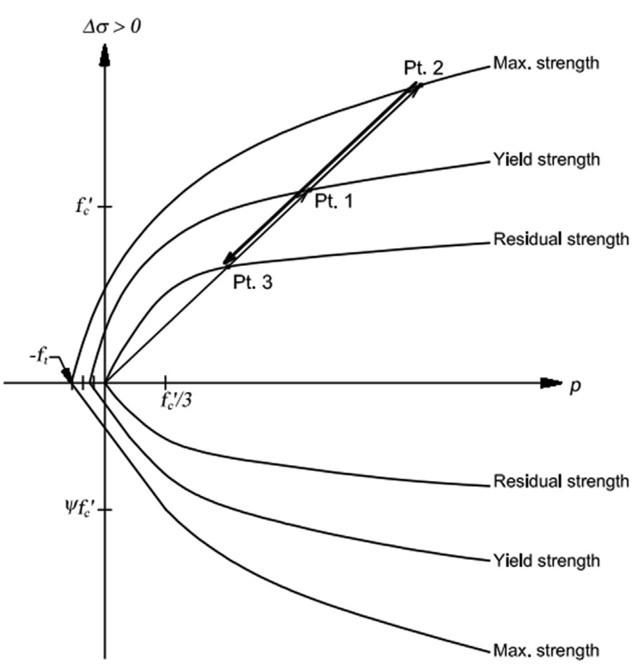

Fig. 7. Three failure surfaces in K&C model.

In the K&C material model, the means of linear interpolation between the two surfaces can be used to determine the current stress limited by the deviatoric stresses. Between the maximum surface and initial yield surface, the current surface is obtained by

$$\Delta\sigma = \eta(\Delta\sigma_m - \Delta\sigma_y) + \Delta\sigma_y \tag{18}$$

and between the residual surface and maximum surface, the current surface is obtained as

$$\Delta\sigma = \eta(\Delta\sigma_m - \Delta\sigma_r) + \Delta\sigma_r \tag{19}$$

where η describes a user-defined function of a modified effective plastic strain measure λ. For hardening, the value of η stays between zero and unity ($\eta(\lambda = \lambda_m) = 1$), then decrease to zero to present softening.

3.2. Damage accumulation

The modified effective plastic strain is defined by the damage functions as

$$\lambda = \begin{cases} \int_0^{\bar{\varepsilon}^p} \frac{d\bar{\varepsilon}^p}{r_f(1+p/r_f f_t)^{b1}} \text{ for } p \geqslant 0, \\ \int_0^{\bar{\varepsilon}^p} \frac{d\bar{\varepsilon}^p}{r_f(1+p/r_f f_t)^{b2}} \text{ for } p < 0. \end{cases} \tag{20}$$

where $d\bar{\varepsilon}^p$ stands for the increment of effective plastic strain, presented as $d\bar{\varepsilon}^p = \sqrt{(2/3)\varepsilon^p_{ij}\varepsilon^p_{ij}}$; f_t describes the tensile strength of concrete; r_f is the strain rate enhancement factor; and b_1 and b_2 are the damage scaling parameters for compression and tension, respectively.

3.3. Volumetric damage

The limitation of using the shear damage accumulation in K&C model [4] as above-description is that, if a tri-axial tension test is considered, then the damage accumulation does not occur because the pressure decreases from zero to $-f_t$ with no deviators. To overcome this drawback, a volumetric damage increment is added to the deviatoric damage whenever the stress path is close to the tri-axial tensile path. A ratio of $|\sqrt{3J_2}/p|$ is measured to be close to this path. The incremental damage now is multiplied by a factor f_d, given by

$$f_d = \begin{cases} 1 - \frac{|\sqrt{3J_2}/p|}{0.1}, & 0 \leqslant |\sqrt{3J_2}/p| < 0.1, \\ 0 & |\sqrt{3J_2}/p| \geqslant 0.1. \end{cases} \tag{21}$$

An increment of the modified effective plastic strain is expressed by

$$\Delta\lambda = b_3 f_d k_d(\varepsilon_v - \varepsilon_{v,yield}) \tag{22}$$

where b_3 is a damage parameter; k_d is the internal scalar multiplier; ε_v and $\varepsilon_{v,yield}$ are the volumetric strains at current and at yield, respectively.

3.4. Governing volumetric behavior

The volumetric behavior of this material model is governed by a pressure-volumetric strain curve, described by a function of tabulated compaction equation of state (EOS), expressed as

$$p = C(\varepsilon_v) + \gamma T(\varepsilon_v)E \tag{23}$$

where p presents the current pressure; $C(\varepsilon_v)$ describes the tabulated pressure evaluated along a 0.0 K isotherm; ε_v is the volumetric strain; $T(\varepsilon_v)$ is the tabulated temperature-related parameter; γ is the specific heat ratio, and E stands for the internal energy. The pressure versus volumetric strain curve describing the tabulated compaction EOS is shown in Fig. 8.

4. Calibration of K&C material model

The latest release of K&C model was implemented as MAT072r3 material model [31] in LS-DYNA. It was initially developed for concrete material subjected to intensive dynamic loads. A total of 49 input parameters which are defined by the user is included in this model. This section presents a calibration of input parameters for FRC based on the test data. The parameters on (1) failure surfaces, (2) dynamic enhancement factors, (3) damage function, (4) equation of state function, and (5) damage evolution are determined.

4.1. Failure surfaces parameters

The plastic behavior of the FRC material is defined based on three independent strength surfaces as discussed above. The failure surfaces parameters are determined using the unconfined compression and tri-axial compression tests with different confining pressures. In this study, a series of compressive tests of FRC under active confining pressures, conducted by Gholampour and Ozbakkaloglu [17] is used. Two grades of compressive strength consisting of 50 and 100 MPa were tested, covering a wide range of FRC used in the real construction. The calibration procedure presented in the work of Markovich et al. [6] is adopted in this process.

Fig. 9 shows the test data of axial stress-strain relationship with different levels of confining pressures of 0, 5, 10, 15, and 25 MPa. Four FRC mixes, which are C100-2, C100-1, C50-2, C50-1 and using two different grades i.e. 100 and 50 MPa of compressive strength and containing hooked fibers at two volume ratios of 1% and 2% are presented.

Based on the stress-strain curves shown in Fig. 9, the yield strengths, maximum strengths, and residual strengths are defined. It can be observed from the test data that as confining pressure increases, compression strength increases, and the ductility also increases significantly. For the normal concrete, it is suggested that the linear line can be assumed to be up to 0.33–0.65 of the unconfined compressive strengths. In this study, the initial yield point is taken at 0.65 of the maximum strength as suggested in the work of Markovich et al. [6]. The residual strength is obtained at a large strain where the stress is slightly changed. Figs. 10–12 show the yield points, maximum points, and residual points and their corresponding fitting curves, respectively. It is noted that since the lateral and the radial stresses in tri-axial compression of cylinders are equal, the pressure (p) in Figs. 10–12 can be determined by

$$p = \frac{1}{3}(\sigma_1 + \sigma_2 + \sigma_3) = \frac{1}{3}(\sigma_1 + 2\sigma_2) \tag{24}$$

By fitting the experimental curves with the fit equations in the form of Eqs. (15)–(17), the eight appropriate constants a_{ij} in these equations are obtained for each mix. Fig. 13 shows the three fitting independent strength surfaces for each FRC mixes. While the calculated failure surfaces parameters for four different FRC mixes are summarized in Table 1. For further analysis, the linear interpolation may be made to determine the input parameters for the cases missing the test data using results presented in Table 1.

4.2. Dynamic enhancement parameters

The properties of FRC are significantly influenced by the loading rate as discussed in the previous section. Thus, the strain rate effect is taken into account to obtain accurate and realistic behaviors of structures. The dynamic increment factor (DIF), which is a function of strain rate, is utilized to consider the effect of strain-rate. In this study, the model of Wang et al. [25] is chosen for compression, whereas the model of Park et al. [2] is employed for tension. It is noted that in MAT072r3, the strain-rate enhancement factors are defined in terms of a curve, in which the abscissa defines the effective strain rate while the ordinate defines the strength enhancement. The input data for strain-rate enhancement factors are summarized in Table 2.

4.3. Damage function η (λ)

The damage function $\eta(\lambda)$ is a user-defined function inputted as a series of 13 (η, λ) pairs. This function begins at $\eta(\lambda = 0) = 0$, increases to $\eta(\lambda_m) = 1.0$ at a certain value $\lambda = \lambda_m$, and then decrease to $\eta = 0$ at some large value of λ. In fact, it is noted in [4] that there are no internal checks to ensure that the user's input handles these specific values. Therefore, at the beginning of the subroutine, the value $\lambda = \lambda_m$ can be defined as the value that corresponds to the value of $\eta = 1.0$. Then, if $\lambda \le \lambda_m$, the current surface is able to be interpolated between the initial yield and the maximum strength. Conversely, whenever $\lambda > \lambda_m$, the current surface can be interpolated between the maximum and the residual strength.

For the convenience of defining the input pairs, Kong et al. [8] proposed a function to describe the relationship between η and λ as

$$\eta(\lambda) = \begin{cases} \alpha\lambda/\lambda_m + (3-2\alpha)(\lambda/\lambda_m)^2 + (\alpha-2)(\lambda/\lambda_m)^3, \ \lambda \leqslant \lambda_m \\ \textit{strain hardening}, \\ \frac{\lambda/\lambda_m}{\alpha_c(\lambda/\lambda_m - 1)^{\alpha_d} + \lambda/\lambda_m}, \ \lambda > \lambda_m \ \textit{strain softening} \end{cases} \tag{25}$$

where α, α_c, and α_d are the constants which govern the strain hardening and softening stages, respectively. The value $\alpha = 3.0$, $\alpha_c = 0.29$, $\alpha_d = 1.86$, and $\lambda_m = 0.000087$ were suggested based on the large amount of trial-and-error calculations.

In this study, based on fitting with the test data, the value $\lambda_m = 0.0006$ is obtained. Fig. 14 shows the η-λ curve of this

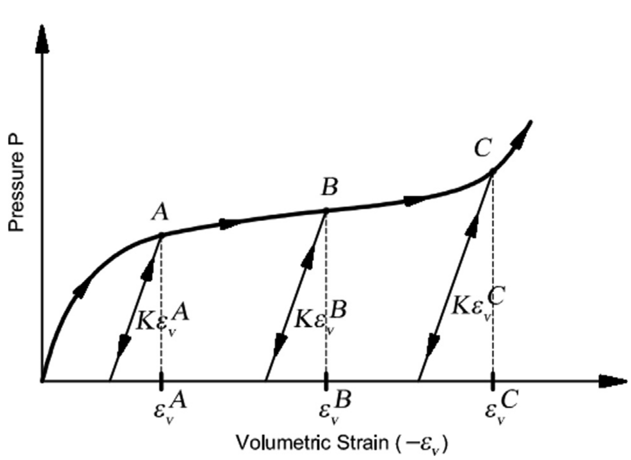

Fig. 8. Tabulated compaction EOS.

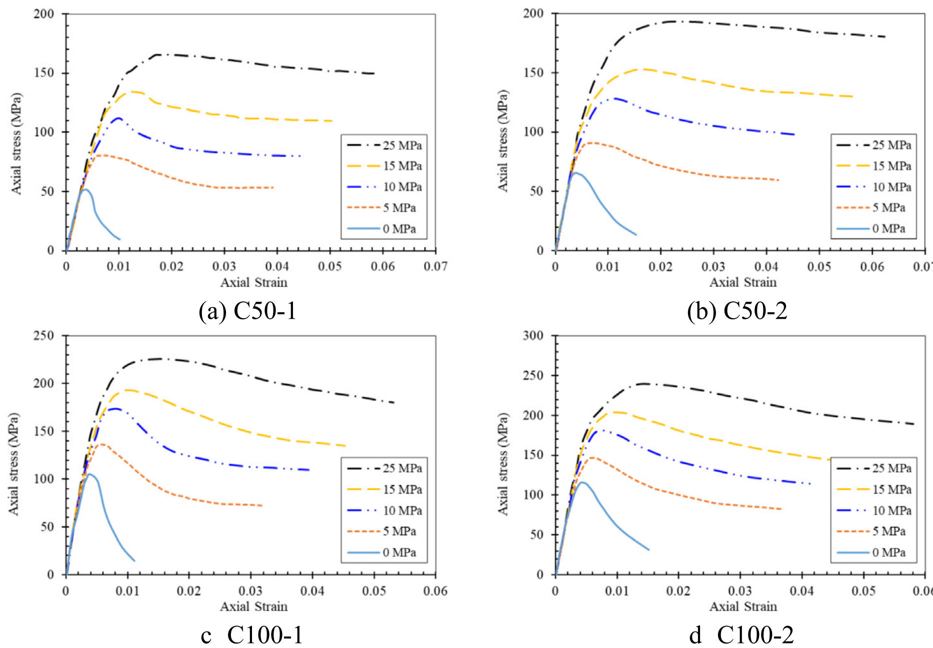

Fig. 9. Axial stress-strain relationships with different confinement levels.

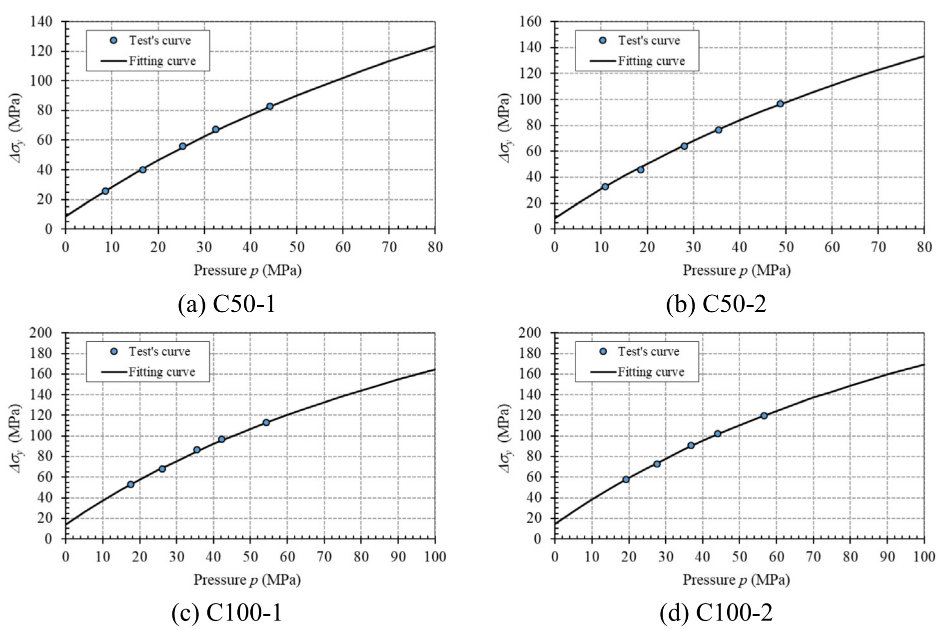

Fig. 10. Yield points of different mixes.

calibration in compared to the automatically generated curve by MAT072r3 model and Kong's curve, while the input series of 13 (η, λ) pairs are presented in Table 3.

4.4. EOS input data

In LS-DYNA, the EOS used for MAT072r3 material model is EOS 8 or the tabulated compaction equation of state [31]. Ten pairs of data points are required for input to define the equation of state function. Since the structures are assumed to work in a normal temperature condition, the effect of heat may be neglected. Due to the insufficiency of test data on the pressure-volumetric strain curve of FRC, a modified curved from [32] is adopted in this study, as shown in Fig. 15. The initial segment of the EOS curve presents a linear response governed by the elastic buck modulus (K_v), which can be determined as the function of elastic modulus (E_c), expressed as

$$K_V = \frac{E_c}{3(1-\nu)} \tag{26}$$

in which ν presents the Poisson's ratio.

The elastic modulus of FRC can be determined by using the empirical equation which was proposed by Lee et al. [14] and expressed as

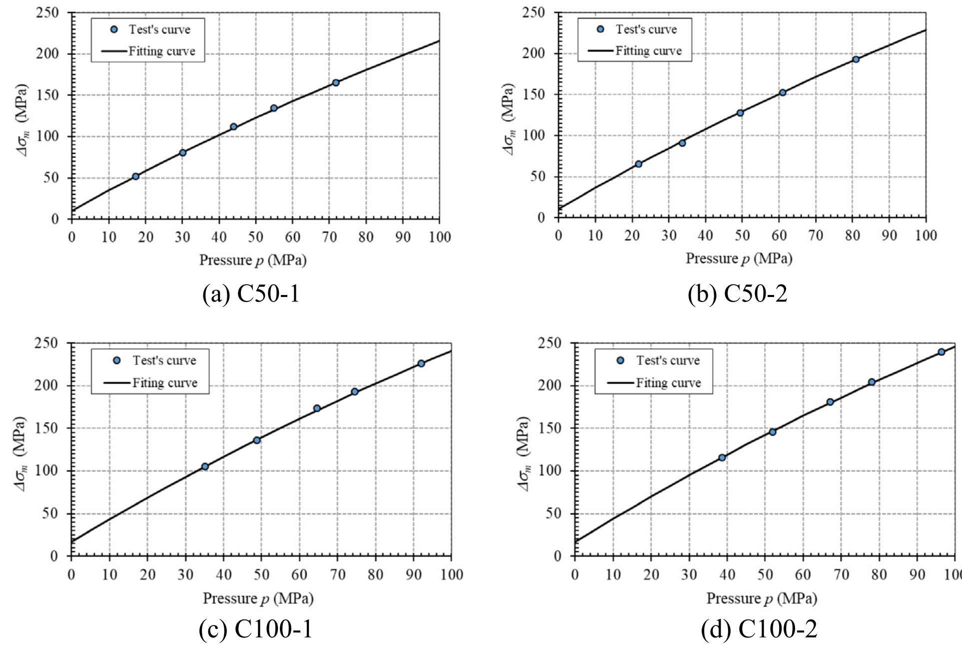

Fig. 11. Maximum points of different mixes.

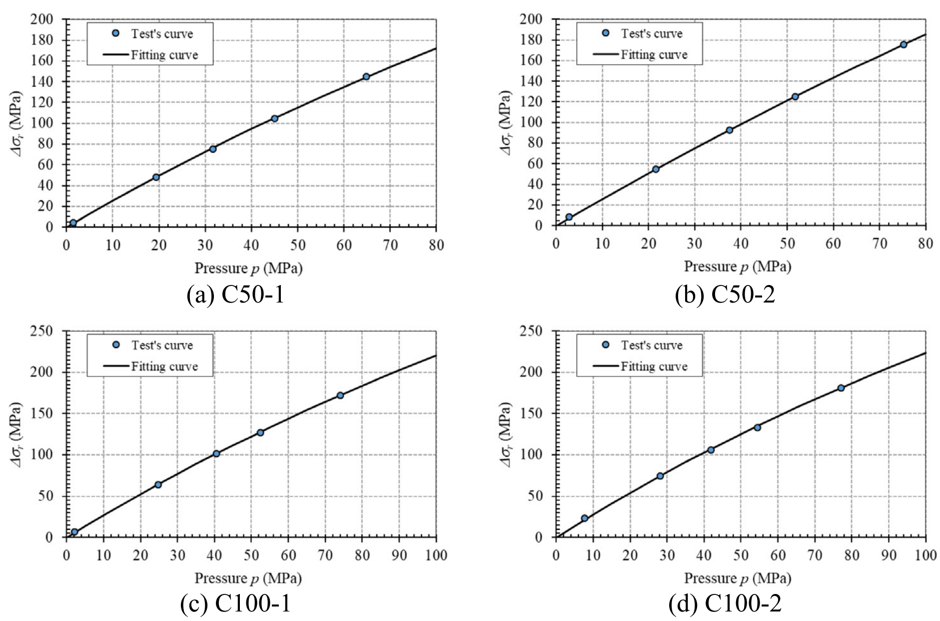

Fig. 12. Residual points of different mixes.

$$E_c = \left(-367V_f\frac{l_f}{d_f} + 5520\right)f_c'^{0.41}, \tag{27}$$

where V_f is the fiber volumetric ratio; f'_c is the compressive strength of FRC; l_f and d_f are the length and diameter of the fiber, respectively.

4.5. Damage evolution parameters

The damage parameter b_1 governs the softening in compression, while the two damage parameters b_2 and b_3 describes the softening in the tension of the uniaxial and tri-axial tensions, respectively. It is noted that the value of these damage parameters depends on the FE mesh size. To eliminate the mesh dependence, the energy from the stress-strain curve underneath should be forced to be equal to G_f/h, in which h is the FE size *and* G_f is the fracture energy. It is suggested that the mesh size h should be equal to the localization width or crack-front length, i.e., the length of the crack on the element surface, which regularly equals to 1–6 times the aggregate maximum size. In the typical simulation, the localization width is chosen together with fracture energy. Thus, damage parameters can be obtained by calculating iteratively until the integration of the stress-strain curve coincides with G_f/h. In fact, unlike the normal concrete, fracture energy of FRC is not given, therefore, other relevant experimental data are used to find out the value of these damage parameters. The calibrated values of the damage evolution parameters are discussed in Section 5.

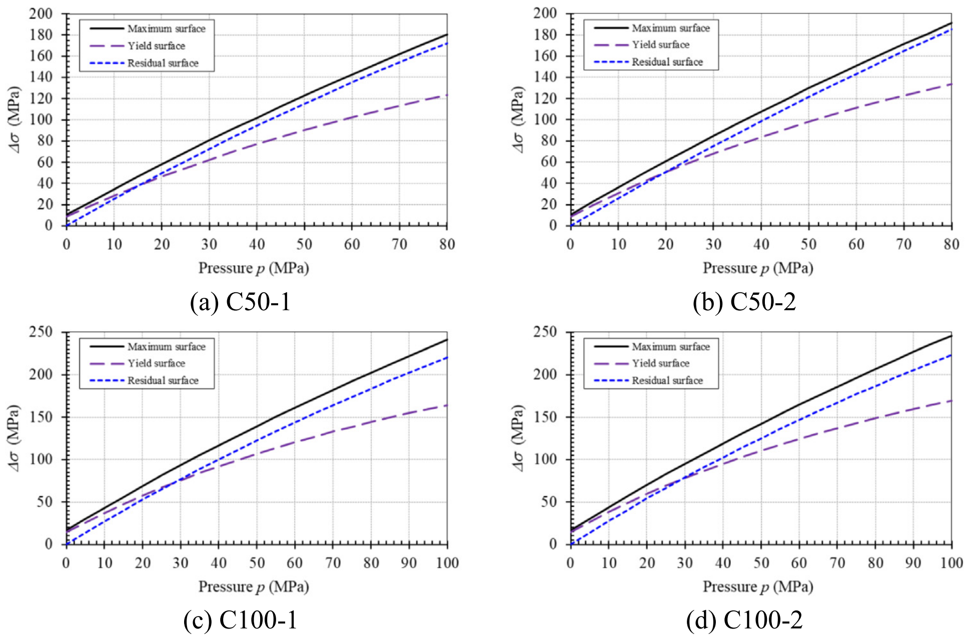

Fig. 13. Three independent strength surfaces for each FRC mixes.

Table 1
Calculated failure surface parameters for FRC mixes.

FRC mix	Failure surfaces parameters*							
	a_0	a_1	a_2	a_{0y}	a_{1y}	a_{2y}	a_{1f}	a_{2f}
C50-1	10.32	0.40181	0.00085	8.46	0.47128	0.00281	0.38268	0.00102
C50-2	10.65	0.38116	0.00078	8.68	0.42427	0.00270	0.38047	0.00064
C100-1	16.68	0.37027	0.00076	14.26	0.41249	0.00254	0.36272	0.00091
C100-2	16.86	0.36115	0.00075	14.64	0.39822	0.00248	0.35097	0.00096

* The unit used for the strength of FRC is MPa.

Table 2
Defined rate enhancement factors.

Strain rate	DIF	Strain rate	DIF
−1000	3.60	0	1.00
−500	3.09	0.00001	1.04
−100	1.90	0.0001	1.08
−53	1.33	0.001	1.12
−30	1.32	0.01	1.16
−20	1.31	0.1	1.21
−10	1.29	1	1.25
−1	1.25	10	1.30
−0.1	1.20	20	1.32
−0.01	1.15	30	1.60
−0.001	1.10	50	1.94
−0.0001	1.05	100	2.53
−0.00005	1.03	500	4.66
0	1.00	1000	6.07

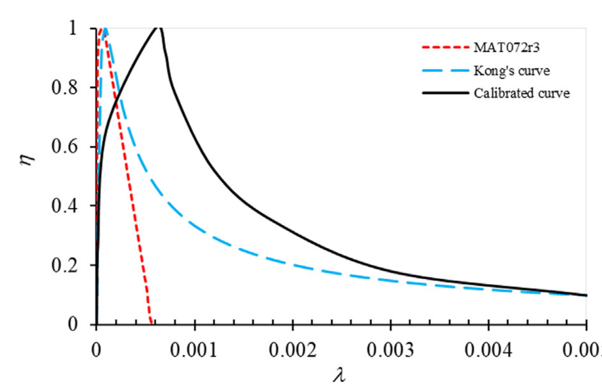

Fig. 14. Comparison of damage functions (η-λ).

5. Numerical results and discussion

5.1. Static compression test

a) FE modeling

In this sub-section, a compression test of FRC specimen conducted by Lee et al. [14] is adopted and analyzed to assess the performance of the calibrated model on describing the compressive behavior of FRC. The 150 mm-diameter by 300 mm-height cylindrical specimen was tested. The specimen used hooked fibers with the length to diameter ratio l_f/D_f = 63.6, 1% of the volumetric ratio and the design compression strength f'_c = 50 MPa. Static compressive test with loading speed of 0.4 mm/min was conducted. Other properties of FRC presented in [14] are utilized to determine the material model input parameters.

The FRC specimen is modeled by the eight-node solid element. Since the parametric analyses of Lin and Gravina [9] showed that the mesh size in the range of 5 mm to 25 mm is appropriated for the similar simulation, the mesh size of approximately 10 mm is used in this simulation. The bottom side of the specimen is fixed by the axial movement resistance boundary condition, while by using displacement control, the force is added to the top of the

Table 3
Input parameters of damage function.

Fair no.	λ	η
1	0	0.000
2	5.0e-6	0.200
3	1.0e-5	0.250
4	1.0e-4	0.660
5	6.0e-4	1.000
6	7.0e-4	0.920
7	8.0e-4	0.780
8	1.2e-3	0.520
9	1.8e-3	0.350
10	3.0e-3	0.180
11	5.0e-3	0.099
12	1.0e0	0.001
13	1.0e10	0.000

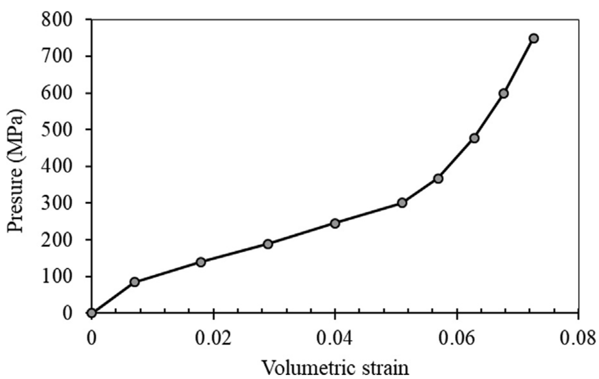

Fig. 15. Modified pressure vs. volumetric strain curve for EOS.

specimen. Static analysis solver of LS-DYNA is employed to ensure that no rate effect occurs on the compressive behavior of FRC.

b) Analysis results and discussion

The stress-strain curves of finite element analysis (FEA) results and the test data are shown in Fig. 16. It is noted that the ascending branch and the ultimate strength of the stress-strain curve are controlled by the parameters of failure surfaces and the damage function (λ,η) calibrated in Section 4. It is shown that with this branch, the FEA results well agree with the test data. Whereas, the softening curve was controlled by the damage parameter b_1. Parametric analyses with different damage parameters b_1 ranging from 0.2 to 1.0 have been carried out and the corresponding results are presented by the dashed lines in Fig. 16. The numerical results reveal that damage parameter b_1 = 0.53 is the best choice for fitting the FEA curve with the test data. In other words, with b_1 = 0.53, the FEA provides a reasonable result on the static unconfined compressive behavior of FRC.

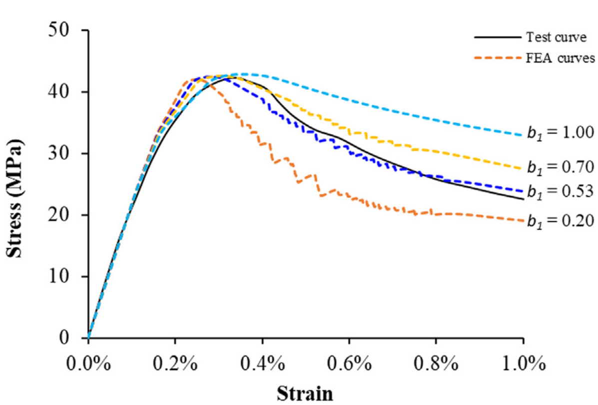

Fig. 16. Comparison of stress-strain curves.

5.2. Static flexural test

a) FE modeling

Fig. 17 shows the geometry of the flexural test of FRC beam conducted by Kim et al. [33]. The FRC beam size was 100 × 100 × 350 mm with 300 mm of the clear span. Hooked fibers with the length to diameter ratio l_f/D_f = 78.9 and volumetric ratio of 1.2% were used. The matrix used for specimen had a compression strength f'_c = 56 MPa. ASTM standard C 1609/C was employed for the test and the net displacement rate was taken as 0.25 mm/min.

The eight-node solid element with the 10 mm mesh size is employed again for this specimen. The input parameters are generated using the material properties presented in [33]. Static analysis solver of LS-DYNA is also applied to ensure no rate effect on compressive behavior of FRC.

b) Analysis results and discussion

As discussed in sub-section 4.5, the two damage parameters b_2 and b_3 govern the tension softening of the uniaxial and tri-axial tensions, respectively. The b_2 effect on the load-deflection behavior of FRC is shown in Fig. 18. It is noted that when b_2 is changed, the value of b_3 keeps constant as b_3 = -5.0. As can be observed here, b_2 is very sensitive to the load-deflection behavior of the material. When b_2 takes a conventional value, i.e. about 2.0, the softening part suddenly drops soon after the curve reaching the ultimate point. This phenomenon describes the behavior of conventional concrete, but not FRC. It is known that due to the effect of fiber, the flexural test of FRC specimen exhibits deflection-hardening behavior. This behavior can be governed by decreasing b_2 from 2.0 to −50. However, it is hard to fit the test curve since K&C model is initially developed for conventional plain concrete, which does not exhibit hardening behavior like FRC.

On the other hand, the damage parameter b_3 has an unclear influence on the softening behavior of FRC, as presented in Fig. 19. In this case, the value of b_3 is changed from 2.0 to −50 while the value b_2 keeps constant as b_2 = −30. Obviously, b_3 can only affect the tri-axial tensile softening behavior, which may not exhibit on the flexural test of a single FRC specimen as discussed in this case. Therefore, based on the parametric analysis, a value of b_3 = −5.0 is recommended to use for flexural analysis of FRC beam under static bending load.

Although deflection-hardening behavior of FRC under bending load can be controlled by changing parameter b_2, however, a good

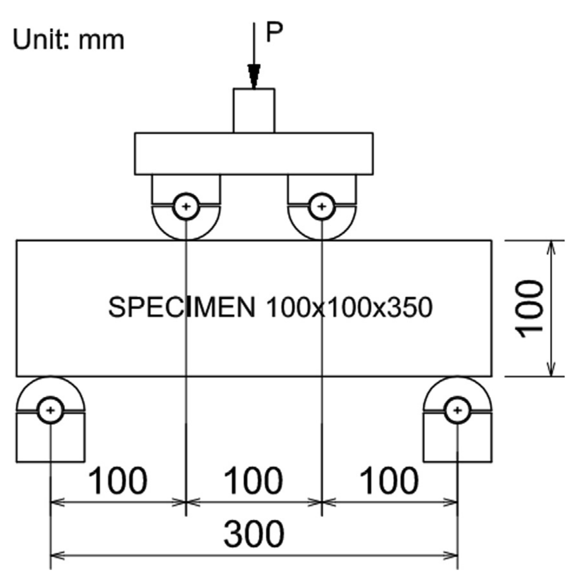

Fig. 17. Flexural test setup.

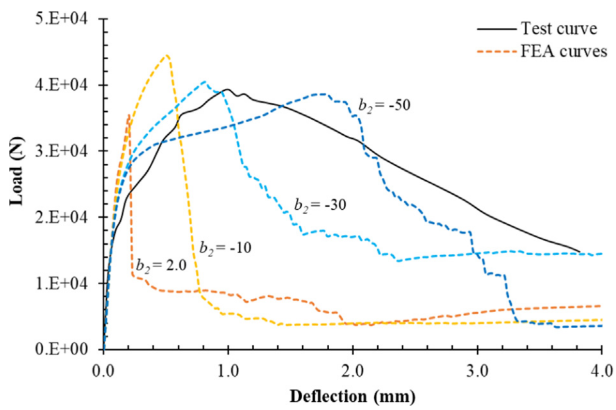

Fig. 18. Effect of parameter b_2.

fitting of the analysis curves and the experimental curve is not achieved. This because the K&C model is initially developed only for conventional plain concrete, which has neither hardening behavior nor ductility in tension. It is only possible to approximate the flexural behavior of FRC using the K&C model, but still limited accuracy. Fig. 20 shows a comparison between FEA results and test data. The FEA curve with using the conventional parameters is presented by the dashed line, while the blue continuous line describes the FEA curve with using the combination of b_2 = −50 and b_3 = −5.0. The comparison indicates that the FEA-calibrated curve is relatively matched with the test data even if tolerance is existing. Also, the calibrated-based model shows to be much more improved compared with the conventional-based model.

Even though the K&C material model cannot accurately describe the flexural resistance (and possibly tensile) behavior of the FRC structure, but the damage behavior of the beam can be simulated very well compared to the experiment result, as presented in Fig. 21. A major crack occurs right under one of the two load points in both test and FEA result (Fig. 21b), whereas the local damage due to compression occurs under the load points in both test and FEA result (Fig. 21c). This highlights that the calibrated K&C model is capable of modeling the damage pattern of the actual FRC beam under bending load.

5.3. Structural behavior of FRC column under blast loading

a) FE modeling

To evaluate the dynamic performance of the calibrated material model, a numerical analysis is implemented for an FRC column subjected to blast loading. For this purpose, the analysis uses one

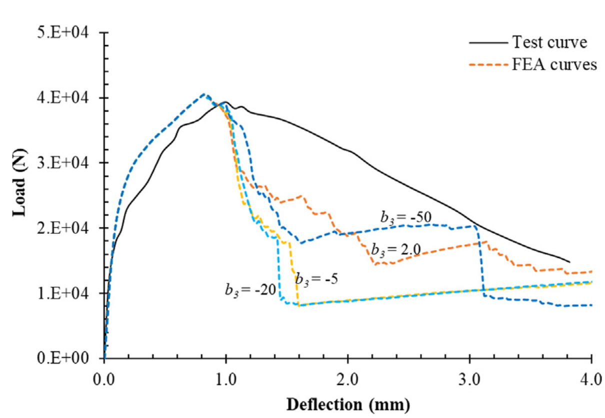

Fig. 19. Effect of parameter b_3.

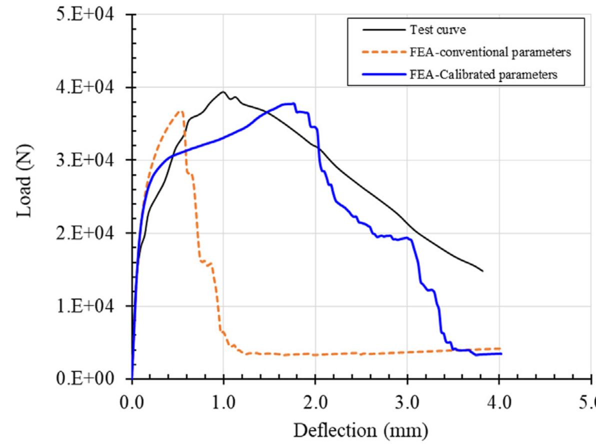

Fig. 20. Comparison of load-deflection curves.

of the blast tests on the FRC column using a shock tube facility in the University of Ottawa, conducted by Burrell et al. [34]. The test specimen had a total length of 2468 mm and a cross-section of 152 × 152 mm as detailed in Fig. 22. Four ϕ11.3 mm longitudinal rebars and ϕ6.6 mm stirrups with a spacing of 75 mm were installed in the column. The column used FRC with ZP-305 hooked fibers and a volumetric ratio of 1.0%. The yield strength of longitudinal and transverse reinforcements was 483 MPa and 604 MPa, respectively while the compressive strength of FRC was 46.1 MPa.

The column was clamped to the support system with a clear span of 1980 mm. The axial compressive load of 294 KN was initially applied to the top of the column. It corresponds to 30% of the compression capacity of the FRC column. The blast-like pressure was horizontally applied to the column using the shockwave system through the steel test frame. In this analysis, the Blast 3 used in the test of Burrell et al. [34] is selected in order to investigate both deformation and damage of the column.

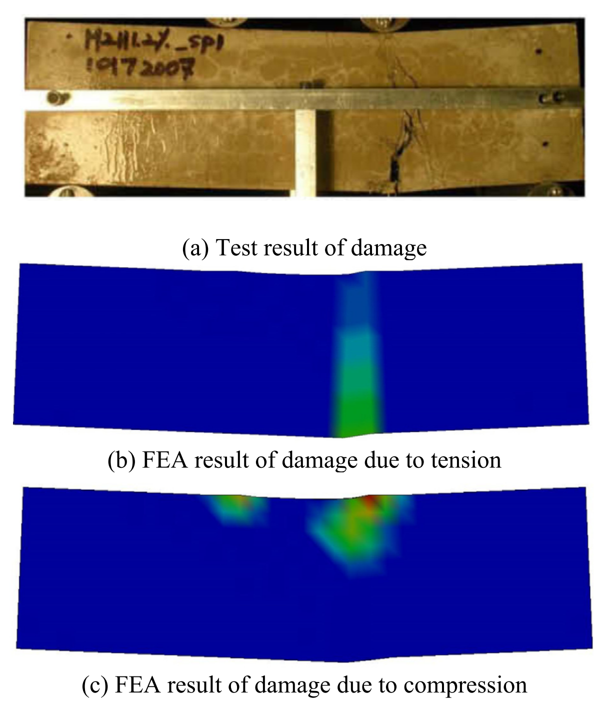

Fig. 21. Comparison of damages.

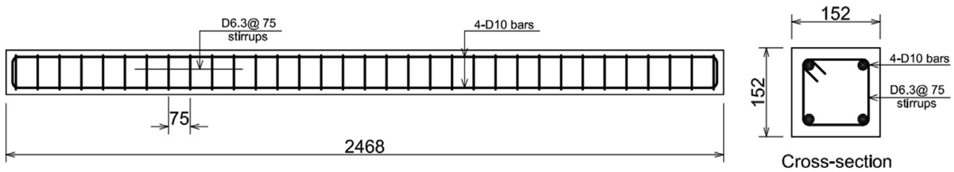

Fig. 22. Detail of specimen (unit: mm).

Table 4
Comparison of maximum displacement at the middle column.

Method	Load	Max. mid-span displacement
Test	Blast No.3	87. 7
FEA	Blast No.3	87.05
Difference	–	*0.75%*

The solid element is used for FRC. The longitudinal and transverse reinforcements are modeled using beam elements. Whereas, the shell element is employed to model the steel frame and steel support system. The modeling uses the mesh size of approximately 10 mm. The dynamic analysis solver of LS-DYNA is applied in this simulation.

b) Analysis results and discussion

Table 4 presents a comparison of the maximum mid-span displacement between the test data and analysis result. It can be seen that the FEA model predicts the maximum displacement of the FRC column accurately with a very small difference of 0.75%. Moreover, the FEA model is also reliable in predicting the failure mechanism of the FRC column, as shown in Fig. 23. Both test and FEA results exhibit the plastic hinges occurring at the end and middle of the column. In addition, the local damage with the expansion of plastic zones induced by the fiber, which are captured from FEA results, as shown in Fig. 23b (in tension zone) and Fig. 23c (in compression zone), agrees well with the test result, as shown in Fig. 23a.

It is noted that all material properties for FRC used in this analysis is accordant with the design guideline for structural application of FRC [35], which is applied in conjunction with EN 19921-1 [36]. According to aforesaid design guideline, the ultimate limite state is reached if in the critical section of the structure, (1) the critical strain of the FRC or, (2) the critical strain of steel rebar reinforcement or, (3) the critical strain of the concrete is reached. For FRC material with the compressive strength is equal to 46.1 MPa, which is used in this analysis, the critical strain in tension is 25‰ and in compression is 3.5‰. According to the analysis result of strain as shown in Fig. 23, the zones where the tensile strain reaches 25‰ and the compressive strain reaches 3.5‰ are failure. Moreover, the tensile strain of steel reinforcement in the critical section is found to reach 25‰ indicating that it is also failure. It can be concluded that analysis result of local damage of the column are in accordance with the test result.

Thus, it is important to conclude that the FEA modeling with the calibrated material model is highly efficient for simulating the failure mechanism and local damage of the FRC column under blast loading. Thus, this proposed calibrated model can be readily applied for both static and dynamic analyses of the FRC structures.

6. Conclusions

An adequate calibration on K&C material model is proposed to model the structural behavior of FRC structures under both static and dynamic loading conditions. Various experimental data on tension, compression, and high-rate behaviors of FRC material using axial and tri-axial tests are used to generate the input parameters. Numerical simulations of different specimens are

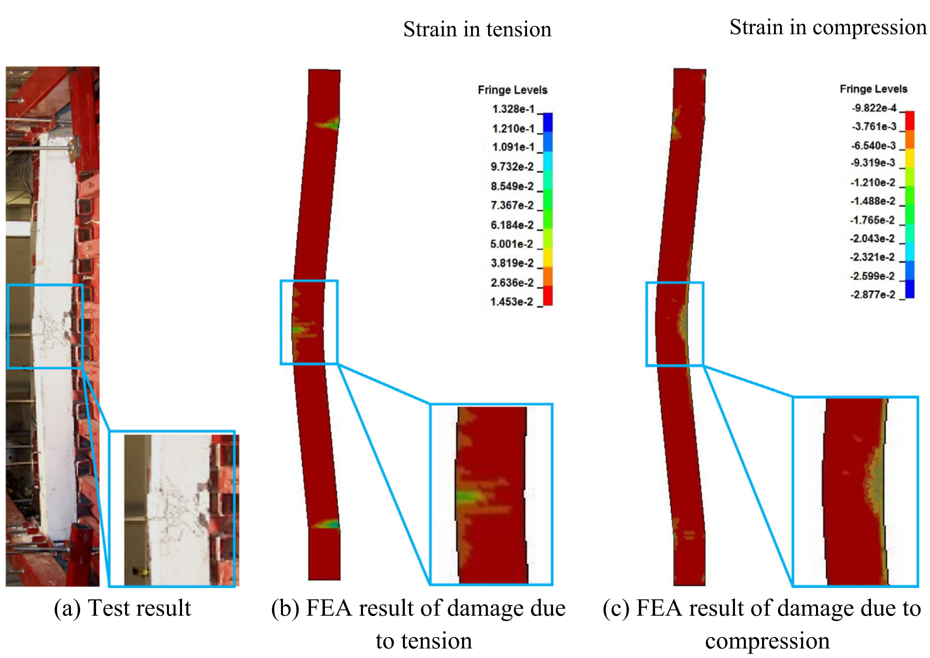

Fig. 23. Comparison of the failure mechanism of the column.

implemented to evaluate the performance of the calibrated material model. From this study, the following conclusions can be drawn.

(1) Obviously, structural behavior of FRC is different from the conventional concrete. Through this study, most of the input parameters that represent the structural behavior of materials such as failure surfaces, dynamic enhancement, EOS input, damage function, and damage evolution parameters need to be calibrated based on the relevant and adequate test data. The calibrated parameters provided in this paper can be used for SFRC which has the volumetric ratio up to 2.0% and compressive strength up to 100 MPa. Other failure surface parameters can be obtained by the given parameters interpolation calculated and provided in this study.
(2) The calibrating procedure presented in this study can be applied to other concrete-like materials. In those cases, relevant experimental data on axial and tri-axial, dynamic, volumetric, and damage behaviors of the material are required.
(3) To evaluate the performance of the calibrated model in simulating the damage of the FRC structures, the design guideline for structural application of FRC applied in conjunction with EN 1992-1-1 is used. It is revealed that analysis results of failure compared to the design criteria in that code are in accordance with the test results.
(4) The calibrated model can be accurately used to present the compressive behavior and the dynamic response of structures. However, owing to the fact that the K&C model was initially developed for the conventional concrete, which does not include the parameter that directly governs the material tensile behavior, resulting in a significant deviation in describing the tensile behavior of the FRC structure. In a further study, this problem should be addressed.

CRediT authorship contribution statement

Duc-Kien Thai: Conceptualization, Writing - review & editing. **Duy-Liem Nguyen:** Writing - original draft. **Duy-Duan Nguyen:** Visualization.

Declaration of interests

The authors declare that they have no known competing financial interests or personal relationships that could have appeared to influence the work reported in this paper.

Acknowledgments

This work was supported by the National Research Foundation of Korea (NRF) grant funded by the Korea government (MSIT) (No. 2018R1C1B5086385).

References

[1] J.J. Kim, G.J. Park, D.J. Kim, J.H. Moon, J.H. Lee, High-rate tensile behavior of steel fiber-reinforced concrete for nuclear power plants, Nucl. Eng. Des. 226 (2014) 43–54.
[2] J.K. Park, S.W. Kim, D.J. Kim, Matrix-strength-dependent strain-rate sensitivity of strain-hardening fiber-reinforced cementitious composites under tensile impact, Compos. Struct. 162 (2017) 313–324.
[3] Y. Wu, J.E. Crawford, J.M. Magallances, Performance of LS-DYNA concrete constitutive models, in 12th International LS-DYNA User Conference2012: Detroit, US.
[4] L.J. Malvar, J.E. Crawford, J.W. Wesevich, D. Simons, A plasticicty concrete material model for DYNA3d, Int. J. Impact. Eng. 19 (9) (1997) 847–873.
[5] J.M. Magallanes, Y. Wu, L.J. Malvar, J.E. Crawford, Recent improvements to release III of the K&C concrete model, in: 11th International LS-DYNA Users Conference. 2010. Detroit, US.
[6] N. Markovich, E. Kochavi, G. Ben-Dor, An improved calibration of the concrete damage model, Finite Elem. Anal. Des. 47 (2011) 1280–1290.
[7] M.M. Attard, S. Setunge, The stress strain relationship of confined and unconfined concrete, ACI Mater. J. 93 (5) (1996) 432–442.
[8] X.Z. Kong, Q. Fang, Q.M. Li, H. Wu, J.E. Crawford, Modified K&C model for cratering and scabbing of concrete slabs under projectile impact, Int. J. Impact. Eng. 108 (2017) 217–228.
[9] X. Lin, R.J. Gravina, An effective numerical model for reinforced concrete beams strengthened with high performmace fiber reinforced cementitious composites, Mater. Struct. 50 (212) (2017) 1–13.
[10] X. Lin, Numerical simulation of blast responses of ultra-high performance fiber reinforced concrete panels with strain-rate effect, Constr. Build. Mater. 176 (2018) 371–382.
[11] L. Yang, X. Lin, R.J. Gravina, Evaluation of dynamic increase factor models for steel fiber reinforced concrete, Constr. Build. Mater. 190 (2018) 632–644.
[12] F. Bencardino, L. Rizzuti, G. Spadea, R.N. Swamy, Stress-strain behavior of steel fiber-reinforced concrete in compression, J. Mater. Civil Eng. 20 (2008) 255–263.
[13] L. Rizzuti, F. Bencardino, Effects of fibre volume fraction on the compressive and flexural experimental behavior of SFRC, Contemp. Eng. Sci. 7 (2014) 379–390.
[14] S.C. Lee, J.H. Oh, J.Y. Cho, Compressive behavior of fiber-reinforced concrete with end-hooked steel fiber, Materials 8 (2015) 1442–1458.
[15] A.S. Ezeldin, P.N. Balaguru, Normal and high strength fiber reinforced concrete under compression, ASCE J. Mater. Civil Eng. 4 (1992) 415–429.
[16] M. Nataraja, N. Dhang, A. Gupta, Stress-strain curves for steel-fiber reinforced concrete under compression, Cement Concr. Compos. 21 (1999) 383–390.
[17] A. Gholampour, T. Ozbakkaloglu, Fiber-reinforced concrete contraining ultra high-strength micro steel fiber under active confiment, Constr. Build. Mater. 187 (2018) 299–306.
[18] CEB-FIP, Model Code 1990: Design Code, 1993.
[19] J.D. Blunt, C.P. Ostertag, Deflection hardening and workability of hybrid fiber composites, ACI Mater. J. 106 (3) (2009) 265–272.
[20] V. Gribniak, G. Kaklauskas, A.K.H. Kwan, D. Bacinskas, D. Ulbinas, Deriving stress-strain relationships for steel fibre concrete in tension from tests of beams with ordinary reinforcement, Eng. Struct. 42 (2012) 387–395.
[21] D.M. Moreno, W. Trono, G. Jen, C.P. Ostertag, S.L. Billington, Tension stiffening in reinforced high performance fiber reinforced cement-based composites, Cement Concr. Compos. 50 (2014) 36–46.
[22] L. Facconi, F. Minelli, Verification of structural elements made of FRC only: a critical discussion and proposal of a novel analytical method, Eng. Struct. 131 (2017) 530–541.
[23] A.E. Naaman, A Statistical Theory of Strength for Fiber Reinforced Concrete, Massachusetts Institute of Technology, 1972.
[24] Z.L. Wang, Y.S. Liu, R. Shen, Stress-strain relationship of steel fiber-reinforced concrete under dynamic compression, Constr. Build. Mater. 22 (5) (2008) 811–819.
[25] S. Wang, M.H. Zhang, S.T. Quek, Effect of high strain rate loading on compressive behaviour of fibre-reinforced high-strength concrete, Mag. Concr. Res. 63 (11) (2011) 813–827.
[26] Z. Xu, H. Hao, H.N. Li, Experimental study of dynamic compressive properties of fibre reinforced concrete material with different fibres, Mater. Des. 33 (2012) 42–55.
[27] T.K. Tran, D.J. Kim, High strain rate effects on direct tensile behavior of high performance fiber reinforced cementitious composites, Cement Concr. Compos. 45 (2014) 186–200.
[28] S. Wang, H.T.N. Le, L.H. Poh, S.T. Quek, M.H. Zhang, Effect of high strain rate on compressive behavior of strain-hardening cement composite in comparison to that of ordinary fiber-reinforced concrete, Constr. Build. Mater. 136 (2017) 31–43.
[29] X. Sun, K. Zhao, Y. Li, R. Huang, Z. Ye, Y. Zhang, J. Ma, A study of strain-rate effect and fiber reinforcement effect on dynamic behavior of steel fiber-reinforced concrete, Constr. Build. Mater. 158 (2018) 657–669.
[30] L.J. Malvar, J.E. Crawford, K.B. Morrill, K&C concrete material model release III – automated generation of material model input, in: Report to the Defense Nuclear Agency, TR-99-24-B1.2000.
[31] Livermore, LS-DYNA Keyword User's Manual, Version 9712007, California.
[32] M. Unosson, Numerical simulation of penetration and perforation of high performance concrete with 75mm steel projectile., in FOA-R–00-01634-311–SE2000: Virginia.
[33] D.J. Kim, A.E. Naaman, S. El-Tawil, Comparative flexural behavior of four fiber reinforced cementitious composites, Cement Concr. Compos. 30 (2008) 917–928.
[34] R.P. Burrell, H. Aoude, M. Saatcioglu, Response of SFRC columns under blast loads, J. Struc. Eng. 141 (9) (2015) 1–14.
[35] T. Kasper, H. Stang, P. Mjoernell, L.N. Thrane, L. Reimer, Design guideline for structural applications of steel fibre reinforced concrete, SFRC Consortium (2014).
[36] EN 1992-1-1, Eurocode 2: Design of concrete structures – Part 1-1: General rules and rules for buildings. European Standard, 2004.